



HAL
open science

Conformational landscape and inertial defect of methoxyphenol isomers studied by mm-wave spectroscopy and quantum chemistry calculations

Atef Jabri, Cédric Bray, Gaël Mouret, Robin Bocquet, A. Cuisset, Guillaume Dhont, Francis Hindle, Anthony Roucou, Daniele Fontanari

► **To cite this version:**

Atef Jabri, Cédric Bray, Gaël Mouret, Robin Bocquet, A. Cuisset, et al.. Conformational landscape and inertial defect of methoxyphenol isomers studied by mm-wave spectroscopy and quantum chemistry calculations. *Journal of Chemical Physics*, 2019, 150, pp.104303. 10.1063/1.5089426 . hal-03173780

HAL Id: hal-03173780

<https://hal.science/hal-03173780>

Submitted on 18 Mar 2021






HAL is a multi-disciplinary open access archive for the deposit and dissemination of scientific research documents, whether they are published or not. The documents may come from teaching and research institutions in France or abroad, or from public or private research centers.

L'archive ouverte pluridisciplinaire **HAL**, est destinée au dépôt et à la diffusion de documents scientifiques de niveau recherche, publiés ou non, émanant des établissements d'enseignement et de recherche français ou étrangers, des laboratoires publics ou privés.

Conformational landscape and inertial defect of methoxyphenol isomers studied by mm-wave spectroscopy and quantum chemistry calculations

Cite as: J. Chem. Phys. 150, 104303 (2019); <https://doi.org/10.1063/1.5089426>

Submitted: 18 January 2019 . Accepted: 21 February 2019 . Published Online: 13 March 2019

A. Jabri, D. Fontanari , A. Roucou , C. Bray, F. Hindle , G. Dhont, G. Mouret , R. Bocquet, and A. Cuisset 



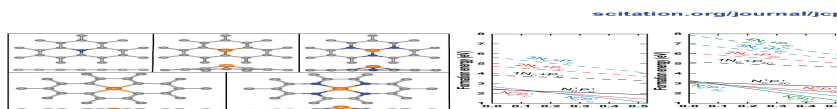
View Online



Export Citation



CrossMark



Volume 150, Issue 10, 14 Mar 2019
Bifunctional mechanism of N, P co-doped graphene for catalyzing oxygen reduction and evolution reactions
J. Chem. Phys. 150, 104701 (2019); doi.org/10.1063/1.5082995
Xiong-Xiong Xue, Li-Ming Tang, Keqiu Chen, Lixin Zhang, En-gu Wang, and Yexin Feng



Conformational landscape and inertial defect of methoxyphenol isomers studied by mm-wave spectroscopy and quantum chemistry calculations

Cite as: J. Chem. Phys. 150, 104303 (2019); doi: 10.1063/1.5089426

Submitted: 18 January 2019 • Accepted: 21 February 2019 •

Published Online: 13 March 2019








View Online



Export Citation



CrossMark

A. Jabri,¹ D. Fontanari,¹  A. Roucou,¹  C. Bray,^{1,2} F. Hindle,¹  G. Dhont,¹ G. Mouret,¹  R. Bocquet,¹
and A. Cuisset^{1,a)} 

AFFILIATIONS

¹Laboratoire de Physico-Chimie de l'Atmosphère, CNRS EA-4493, Université du Littoral Côte d'Opale, 59140 Dunkerque, France

²Université de Bordeaux, Institut des Sciences Moléculaires, F-33400 Talence, France

^{a)}Electronic mail: arnaud.cuisset@univ-littoral.fr. Tel: +33 3 28 23 76 13

ABSTRACT

Because methoxyphenols (MP) are emitted in significant quantities during biomass fires and contribute to the secondary organic aerosols formation which impacts the climate, their gas phase monitoring in the atmosphere is crucial and requires accurate rovibrational cross sections determined with a good knowledge of their ground state (GS) and vibrationally excited state (ES) molecular parameters. Therefore, the rotational spectra of the two isomers, 2-MP (guaïacol) and 4-MP (mequinol), have been measured in absorption and in emission at room temperature using a frequency multiplication chain and a mm-wave Fourier transform chirped-pulse spectrometer, respectively. Guided by quantum chemistry calculations, the conformational landscape has been characterised and the observation of only one rotamer in the spectra of 2-MP and 4-MP has been explained. For 2-MP, the most stable conformation is justified by an intramolecular O–H···OCH₃ hydrogen-bond which has been characterised by a topology analysis of the electron density. In a global fit including more than 30 000 line assignments, rotational and quartic centrifugal constants of the GS and the three lowest energy ES have been determined allowing to reproduce the millimeter-wave spectra at the experimental accuracy. The same work has been performed on the *cis*-rotamer of 4-MP highlighting some perturbations marring the fit quality for two vibrationally ES. Finally, the isomeric dependence of the negative inertial defect ΔI agrees with that of the lowest energy out of plane mode ν_{45} , and the variation of ΔI with the degree of vibrational excitation allows a fine estimation of $\nu_{45} = 1$ vibrational wavenumber.

Published under license by AIP Publishing. <https://doi.org/10.1063/1.5089426>

I. INTRODUCTION

Methoxyphenols are oxygenated aromatic compounds present as building blocks in natural lignin which play a key role in the cellular formation of wood and barks. These biogenic volatile organic compounds (BVOCs) are released in significant quantities during biomass fires (including natural fires and residential wood heating). 2-methoxyphenol (2-MP) and 2,6-dimethoxyphenol commonly named guaïacol and syringol, respectively, are the two main products of lignin pyrolysis with emission rates varying from 0.9 g to 4.2 g per kg of burned vegetation.¹ They are semi-volatile products principally detected in the gas phase and are able to chemically

evolve in the atmosphere via degradation processes. Several studies have been performed in order to determine the kinetics and the reactivity intermediates involved in the tropospheric oxidation processes and the subsequent formation of secondary organic aerosols (SOA) which impact the climate.² It is well established that aromatic oxygenated compounds such as methoxyphenols have a strong potential for the formation of SOA with specific hygroscopic properties depending on the ability to form intermolecular hydrogen bonds.³

Indeed, depending on the isomer and the conformer forms, methoxyphenols, as other BVOCs, may present intramolecular hydrogen bond preventing or not the formation of intermolecular hydrogen bonds (HB) with water or other molecular environments.⁴

In 2-MP, the hydroxyl and methoxy groups in “ortho” position may form an intramolecular HB; whereas, in 3-methoxyphenol (3-MP) and 4-methoxyphenol (4-MP, commonly called mequinol), they are too distant to interact directly through space, which enhances the conformational flexibility and the possibility to observe several stable rotamers. Therefore, the conformational landscape of MP has been the subject of several experimental and theoretical studies^{4–9} showing a clear dependence on the isomeric forms.

Rotationally resolved electronic spectroscopy in molecular beam has provided the most complete conformational analyses on the MP isomers. Unlike 2-MP where UV spectra were assigned to a single conformation stabilised by the formation of an intramolecular HB between the adjacent hydroxyl and methoxy functional groups, several stable conformers depending on the –OH and –OCH₃ relative orientations were identified for 3-MP and 4-MP.^{6,8} Two iso-energetic *cis* and *trans* stable rotamers may be individually identified in 4-MP spectra due to the significant differences of the rotational constants in the ground and electronically excited states. For 3-MP, only 3 of the 4 predicted rotamers were observed and the non-observation of the fourth conformation was explained by the non-planar structure of 3-MP in the electronic singlet state by weakening the electronic transition with an unfavorable Franck-Condon factor.

Recently, our group has demonstrated that the conformational landscape of 3-MP may be fully described at room temperature in the electronic ground state (GS) using mm-wave rotational spectroscopy supported by quantum-chemical calculations.⁹ Compared to the previous UV studies, the mm-wave analysis has revealed the 4 stable conformations theoretically predicted. The GS rotational constants were fitted at the kHz level of accuracy and the complete sets of quartic centrifugal distortion constants were determined. Moreover, pure rotational transitions in the low-frequency vibrational states were assigned and the degree of non-planarity of the MP may be discussed from the experimental inertial defects which are accentuated by the out of plane –OCH₃ bending excitation. This study presents a similar approach on guaiacol (2-MP) and mequinol (4-MP) allowing to discuss the isomerism influence on the conformational landscape of methoxy-aromatic compounds.

II. METHODS

A. Experimental issues

Commercially available MP isomers (2-MP, 3-MP, and 4-MP) with stated purities higher than 98% were purchased from Acros Organics. Further purification was performed by continuous pumping for over 24 h in order to eliminate methanol traces. With room temperature equilibrium vapour pressures of around 10 and 140 μ bar,¹⁰ 2-MP and 4-MP are, respectively, the most and the less volatile MP isomers. The equilibrium MP vapour pressures were directly injected in the gas cell, and a continuous flow at a pressure of 10 μ bar was maintained by a rough pumping.

The room temperature high resolution rotational spectra of the three isomers were measured in the 70–330 GHz spectral range using two spectrometers of the Laboratory of Physical Chemistry of the Atmosphere (LPCA): line by line and broadband measurements were, respectively, performed with the absorption mm-wave spectrometer based on a frequency multiplication chain¹¹ and

the recently developed mm-wave chirped pulse Fourier transform (CPFT) spectrometer.¹²

1. Frequency multiplication chain

The sub-THz spectrometer based on a frequency multiplication chain was described in detail by Mouret *et al.*¹¹ The molecules in gas phase are probed in a 1250 mm-long and 56 mm-diameter stainless steel absorption cell equipped with Teflon windows. The measurements were performed in a double pass configuration by adding a polarizing grid and a rooftop mirror.^{13,9} Two off-axis parabolic mirrors were placed, one before the grid to collimate the radiation into the cell and one after the grid to refocus it on the detector. A zero bias Schottky diode associated with a horn antenna and a liquid helium cooled InSb bolometer were used as detectors in the ranges 70–110 GHz and 140–330 GHz, respectively. A frequency modulation at 13 kHz with a depth in the range of 300–900 kHz was added to the mm-wave source in order to optimize the spectrometer sensitivity. The signal detection was performed by a standard lockin amplifier operating at the second harmonic of the modulation frequency. The individual frequency points were measured with an integration time of 50 ms or 200 ms depending on the absorption intensity with a frequency step of 100 kHz. The baseline arising from Fabry-Pérot effects presents strong amplitude variations and a free spectral range, both approximately 50 times broader than the molecular intensities and linewidths, respectively. These variations were easily removed from the spectra by using a low pass FFT filter as described in Ref. 49. The spectral resolution is limited to 100 kHz since the observed lines are Doppler limited [$\Delta\nu_{\text{Doppler}} \approx 90$ kHz (FWHM)] and artificially broadened by the frequency modulation.¹¹ The experimental error of measured line frequencies was estimated between 70 kHz and 80 kHz using Eq. (2) of Ref. 14 taking into account the averaged S/N ratio, the frequency step and the molecular linewidth.

2. Millimetre-wave chirped pulse Fourier transform spectrometer

A CPFT spectrometer using an amplified multiplier chain covering the band from 190 to 210 GHz was employed. This spectrometer is described in detail in Ref. 12. Briefly, the mm-wave CPFT spectrometer was used with a 1200 mm-long stainless steel cell closed by Teflon windows. The mm-wave was collimated and propagated through the cell by two off-axis parabolic mirrors. The molecular re-emission beam is focused onto the detector by a Teflon lens. The CPFT spectrometer was used in segmented mode as described by Neill *et al.*¹⁵: 23 pulses of 700 ns duration and 1 GHz bandwidth with an overlapping of 100 MHz between each chirped pulse were used to cover the 20 GHz band of the spectrometer. The free induction decay was recorded 20 ns after the end of the excitation pulse (recovery of the amplifier) and during 4 μ s. Fast Fourier transform was employed on the full recorded data with application of Kaiser Bessel windows ($\beta = 8$) for side lobe suppression. The pressure was measured with a 1 mbar full scale pressure gauge (MKS Baratron). All free induction decay signals have been measured at room temperature around 10 μ bar. A comparison of the S/N ratio obtained on 3-MP mm-wave spectra in the 200 GHz frequency region with the two spectrometers is presented in Fig. 1. For a 1 GHz range, the line by line absorption spectrum measured with the frequency multiplication chain and the emission broadband spectrum recorded

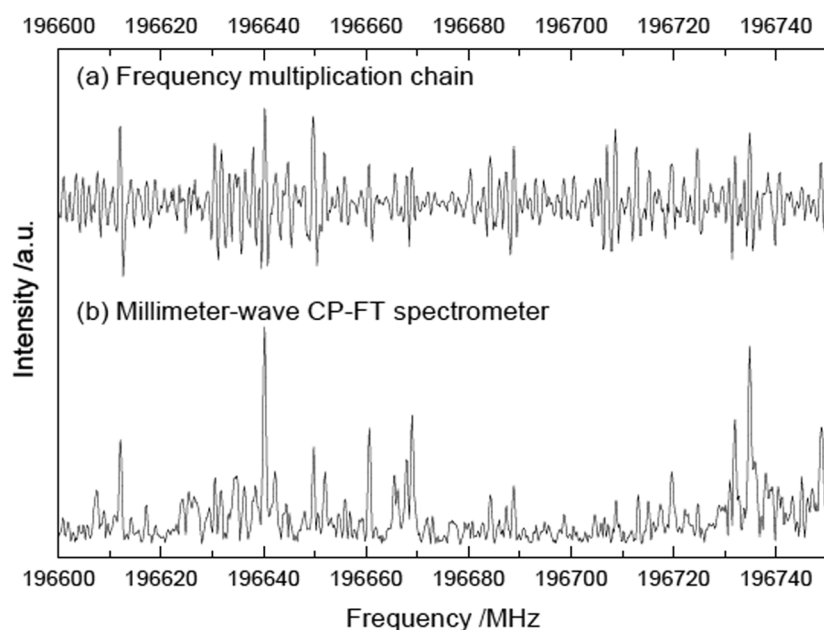


FIG. 1. Comparison between absorption (a) and emission (b) rotational spectra of 3-MP measured at room temperature in the 196.6 GHz–196.75 GHz frequency range with the frequency multiplication chain and the CPFT spectrometer, respectively. For the two spectra, the same acquisition time is used to record 1 GHz ranged rotational spectra in line by line absorption measurements with frequency steps of 200 kHz and time constant of 200 ms and broadband emission measurement with 16 000 000 averaged spectra.

with the CPFT instrument have been obtained with the same acquisition time by adjusting the frequency step to 200 kHz and the time constant to 200 ms for the first spectrometer operating in 2F modulation and by averaging 16 000 000 emission spectra for

the second one. A slight but relevant improvement of the S/N ratio (≈ 1.5) is obtained with the CPFT spectrometer. Then, experimental accuracies of the measured CPFT lines were estimated to 60 kHz and 70 kHz, respectively, in the 190–210 GHz spectral range.

TABLE I. Calculated and experimental GS parameters of observed conformers of guaiacol (2-MP C1) and *cis*- and *trans*-mequinol (4-MP C1 and C2): rotational constants, inertial defects $\Delta I = I_c - I_b - I_a$, and amplitude and orientation of the permanent dipole vector.

Parameter	Unit	Calculation:		Experiment:		
		Reference 6 B3LYP/6–31G(d,p)	This work B3LYP/cc-pVTZ ^a	Reference 6 UV spectroscopy	This work mm-wave spectroscopy	
2-MP C1	A	MHz	2609.8	2621.0	2607.1(1)	2 607.062 60(117)
	B	MHz	1549.8	1557.3	1560.8(1)	1 560.796 45(40)
	C	MHz	978.4	983.0	982.9(1)	982.871 842(199)
	ΔI	amu.Å ²	−3.20	−3.22	−3.46(3)	−3.459 49(27)
	μ	D		2.66		
	$\angle(\vec{\mu}, a)$	°		37.5	28(1) ^b	
4-MP C1	A	MHz	4888.8	4931.5	4880.2(1)	4 879.847 983(75)
	B	MHz	985.1	989.1	990.7(1)	990.884 961(33)
	C	MHz	824.2	828.2	828.5(1)	828.4 395 997(213)
	ΔI	amu.Å ²	−3.22	−3.22	−3.70(3)	−3.555 190(34)
	μ	D		2.40		
	$\angle(\vec{\mu}, a)$	°		89	88(1) ^b	
4-MP C2	A	MHz	4881.9	4925.8	4871.7(1)	
	B	MHz	985.6	989.5	991.5(1)	
	C	MHz	824.3	828.3	828.6(1)	
	ΔI	amu.Å ²	−3.18	−3.20	−3.53(2)	
	μ	D		0.50		
	$\angle(\vec{\mu}, a)$	°		27		

^aEffective rotational constants (including terms due to quartic centrifugal distortion constants).

^bElectronic transition moment measured in Ref. 6.

B. Quantum chemical calculations

High level of theory quantum chemistry calculations were performed using the Gaussian 16 package.¹⁶ As done for 3-MP,⁹ the potential energy surfaces (PES) of 2-MP and 4-MP were built at the B3LYP/6-311++G(d,p) level of theory by scanning with a step of 5° the dihedral angles between the $-\text{OH}$ and $-\text{OCH}_3$ groups and the aromatic plane. Minima and saddle points were calculated with the B3LYP functional and larger Dunning¹⁷ correlation consistent basis set cc-pVTZ with an optimisation process using the tight convergence criteria providing the GS energies, rotational constants, dipole moments of the stable conformers and conformational barriers (see Table I). The B3LYP/cc-pVTZ level of theory has proved one's worth for the computational study on the molecular conformations of phenolic compounds.¹⁸ Anharmonic frequencies have been computed with the same level of theory using an ultrafine grid. Finally, the MOLPRO program,¹⁹ and the Multifunctional Wavefunction Analyser (Multiwfn)²⁰ have been used to evidence the formation of intramolecular H-Bond in 2-MP: with MOLPRO, the 2-MP molecule was optimized in its GS and its wave function generated at the cc-pVDZ level of theory; subsequently, the Multifwn code has been employed to extract the electron density from the corresponding wave function in order to analyse its topology, highlighting critical structures that evidenced, from the standpoint of the quantum theory of atom in molecules, the formation of an intramolecular H-bond.

III. RESULTS AND DISCUSSION

A. Theoretical analysis

1. *Guaïacol (ortho-, 2-MP)*

Figure 2 presents the PES built at the B3LYP/6-311++G(d,p) level of theory describing the conformational space of 2-MP. A deep minimum is observed when the O–H and the O–CH₃ bonds lie in the benzene ring plane with the H atom of the phenol group in the donor position between the two oxygen atoms. This conformer labelled C1 is stabilized by the intramolecular O–H...OCH₃ HB indirectly evidenced via an electronic origin red-shifted compared to phenol in the vibrationally resolved enhanced multiphoton ionization (REMPI) spectrum of Ref. 6 and in the core photoelectron spectra (XPS) of Ref. 4 indicating that the high energy conformers of 2-MP show significant changes when the HB is broken. These higher energy conformers labelled C2 and C3 are identified as minima of the 2-MP PES (Fig. 2) with strongly higher energies compared to C1 (energy differences of 1392 cm^{-1} and 1720 cm^{-1} are, respectively, calculated for C2 and C3 at the B3LYP/cc-pVTZ level of theory). In agreement with the optimised rotamer structures calculated by Islam *et al.*⁴ with a smaller basis set, the C2 conformer exhibits the O–H and the O–CH₃ bonds lying in the *ab* plane but with the hydroxyl group turned 180° compared to C1. In C3, the O–CH₃ bond is out of plane and this higher energy conformer is stabilised by a H–O...HCH₂O longer than the O–H...OCH₃ HB in C1. Two

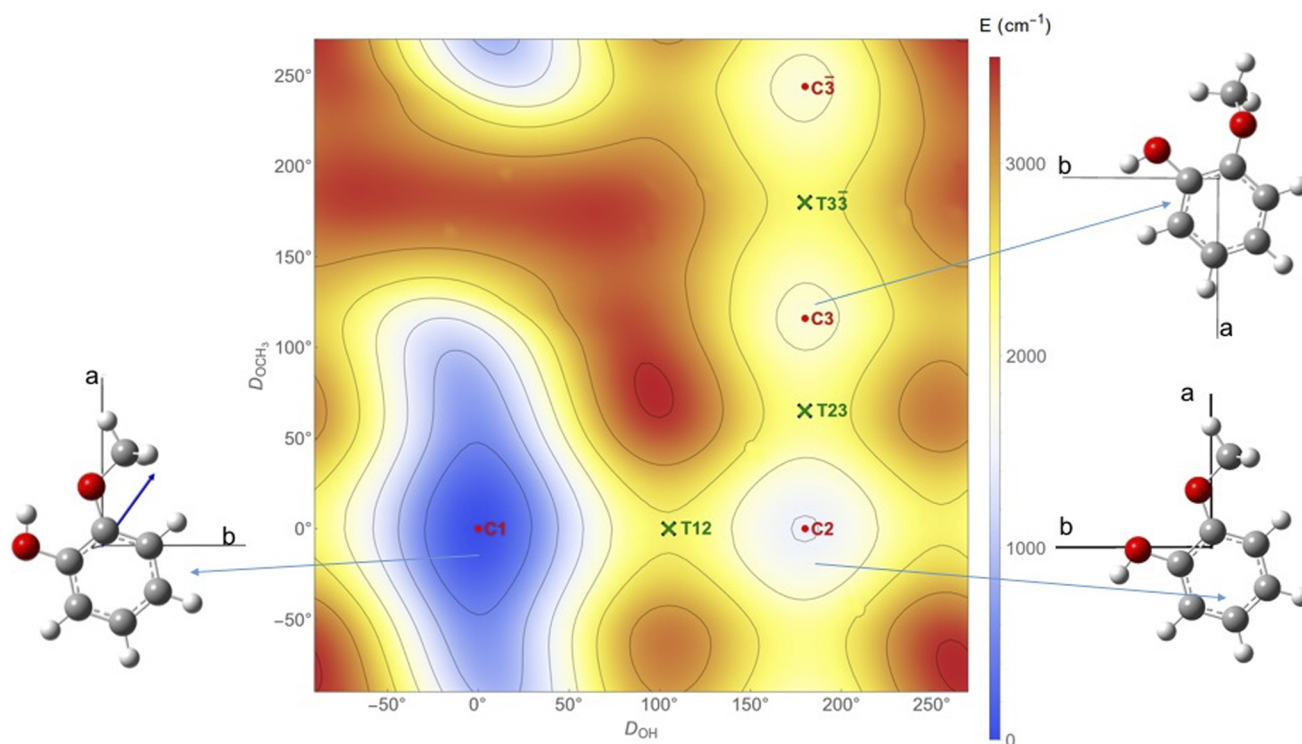


FIG. 2. PES describing the conformational space of 2-MP built with a step of 5° at the B3LYP/6-311++G(d,p) level of theory. Local minima and saddle points are, respectively, marked with a red dot and a green cross. Geometries of C1, C2, and C3 stable conformers are optimized at the B3LYP/cc-pVTZ level of theory shown in the *ab* plane with the permanent dipolar vector (blue arrow) for C1.

isoenergetic minima C3 and its mirror image $\bar{C}3$ are observed in the PES depending on the positions up and down of the methoxy O-CH₃ group in relation to the ab plane. The rotamers C2, C3, and $\bar{C}3$ are too high in energy to be observed at room temperature and only the most stable C1 is expected in the mm-wave spectrum. For this conformer, *a*-type and *b*-type rotational transitions are expected since the permanent dipole moment is oriented in the ab plane with the $|\mu_a|$ and $|\mu_b|$ components estimated, respectively, to 2.1 and 1.6 Debye at the B3LYP/cc-pVTZ level of theory (Table I).

In order to characterize the intramolecular O-H...OCH₃ HB in C1, a topology analysis for electron density was performed following the method described in Sec. II B. The results are presented in Fig. 3 where we have considered the critical points of the positive electron density distribution function of 2-MP. In addition to covalent bonds drawing the 2-MP C1 conformer, the intramolecular O-H...OCH₃ HB appears clearly. The Multifwn analysis shows that the covalent bond critical points have a potential energy density between -0.357 and $-0.798 E_h$, while the O-H...OCH₃ bond has a potential energy density of $-0.022 E_h$, significantly weaker than the covalent energies. This value is characteristic of a moderate intramolecular HB, as it was demonstrated by the computational study of Cesari *et al.* in Ref. 18.

2. Mequinol (*para*-, 4-MP)

The PES of 4-MP shown in Fig. 4 exhibits four minima associated with four stable rotamers C1, $\bar{C}1$, C2, and $\bar{C}2$. Considering the mirror reflexion in a symmetry plane containing the *c*-axis and the two C-O bonds, C1 and C2 are, respectively, equivalent to $\bar{C}1$ and

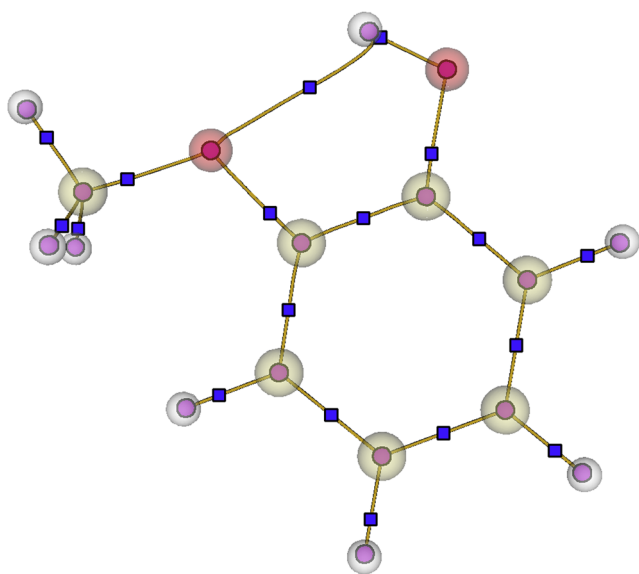


FIG. 3. Topology analysis for electron density on 2-MP C1 optimized at the CCSD/cc-pVDZ level of theory using the Multifunctional Wavefunction Analyser (Multiwfn).²⁰ The full circles, observed at the center of the atoms, represent the atomic critical points corresponding to local maxima in the three perpendicular directions of spaces. The full squares correspond to saddle points (maximum in two directions of space and minimum in the third one) of electron density. The connections between maxima of the electron density via the saddle points are represented with full squares.

$\bar{C}2$ with isoenergetic PES minima. C1 and C2 correspond, respectively, to the *cis*- and *trans*-rotamer of 4-MP. An energy difference $\Delta E = E_{C1} - E_{C2}$ was estimated to 5.7 cm^{-1} with the B3LYP/cc-pVTZ level of theory calculations. Islam *et al.* in Ref. 4 have obtained $\Delta E = 1.4 \text{ cm}^{-1}$ with a smaller 6-311++G** basis-set. For both cases, taking into account the accuracy of density functional theory (DFT) calculations, the difference is too small to be significant and the C1 and C2 conformers of 4-MP may be considered as isoenergetic with equivalent populations in the conformational mixture. The saddle points noted T12 in Fig. 4, calculated around 890 cm^{-1} at the B3LYP/cc-pVTZ level of theory, indicate that the conformational barriers are too high to observe tunneling splitting between C1 and C2 rotamers. As shown in Table I with the GS calculated parameters, the rotational constants and therefore the inertial defects of *cis*- and *trans*-mequinol are very close, whereas their permanent dipoles are strongly different. The module of the C1 permanent dipole moment is 4.8 times longer than the one of C2. *a*-type and *b*-type rotational transitions are predicted for C2 whereas only strong *b*-type transitions are expected for C1. Consequently, the observation of a *b*-type rotational mm-wave spectrum for 4-MP in *cis* configuration is privileged in comparison with an hypothetical observation of the *-trans* 4-MP *a*-type and *b*-type rotational signatures. In Ref. 6, Ruiz-Santoyo *et al.* were able to assign individually rotationally resolved electronic spectra in the S₁ state of the *cis* and *-trans* 4-MP rotamers by exciting the two electronic origin bands separated by around 97 cm^{-1} on the one-color REMPI spectrum.

B. Spectral analysis

Spectral analysis was performed using SPFIT/SPCAT Pickett's programs²¹ where a Watson-type Hamiltonian, describing a semi-rigid rotor model developed up to quartic centrifugal distortion constants, is implemented. We have chosen, in I' representation, the A-reduction for 2-MP and the S-reduction for 4-MP since 4-MP is nearly prolate ($\kappa \simeq -0.92$), whereas 2-MP is strongly asymmetric ($\kappa \simeq -0.3$). The AABS (Assignment and Analysis of Broadband Spectra) package from Kisiel^{22,23} was used for a direct assignment of measured lines to predicted rotational transitions. As for 3-MP,⁹ a specific treatment of the internal rotation of the methyl group was not required in this study. Indeed, the barrier heights hindering the internal rotation for the MP isomers are very high (around 900 cm^{-1}) and the internal rotation splitting could not be resolved as in several cases of methoxy groups attached to benzene rings such as methyl anisole isomers.²⁴⁻²⁶ Pure rotational transitions in the low-energy vibrationally excited states (ES) (typically below 400 cm^{-1})²⁷ were observed in the room-temperature mm-wave spectra. Therefore an analysis of the ES of 2-MP and 4-MP was undertaken subsequent to the GS analysis.

1. GS analysis

The GS rotational transitions of 2-MP were first assigned by comparing the experimental spectrum to the preliminary prediction obtained with the SPCAT program with the pure rotational constants measured in Ref. 6 and the quartic centrifugal distortion constants resulting from our quantum chemical frequency calculations including the analysis of the vibrational-rotational coupling. A 15 GHz portion of the measured mm-wave spectra highlighting the huge density of lines and the results of the spectral analysis of

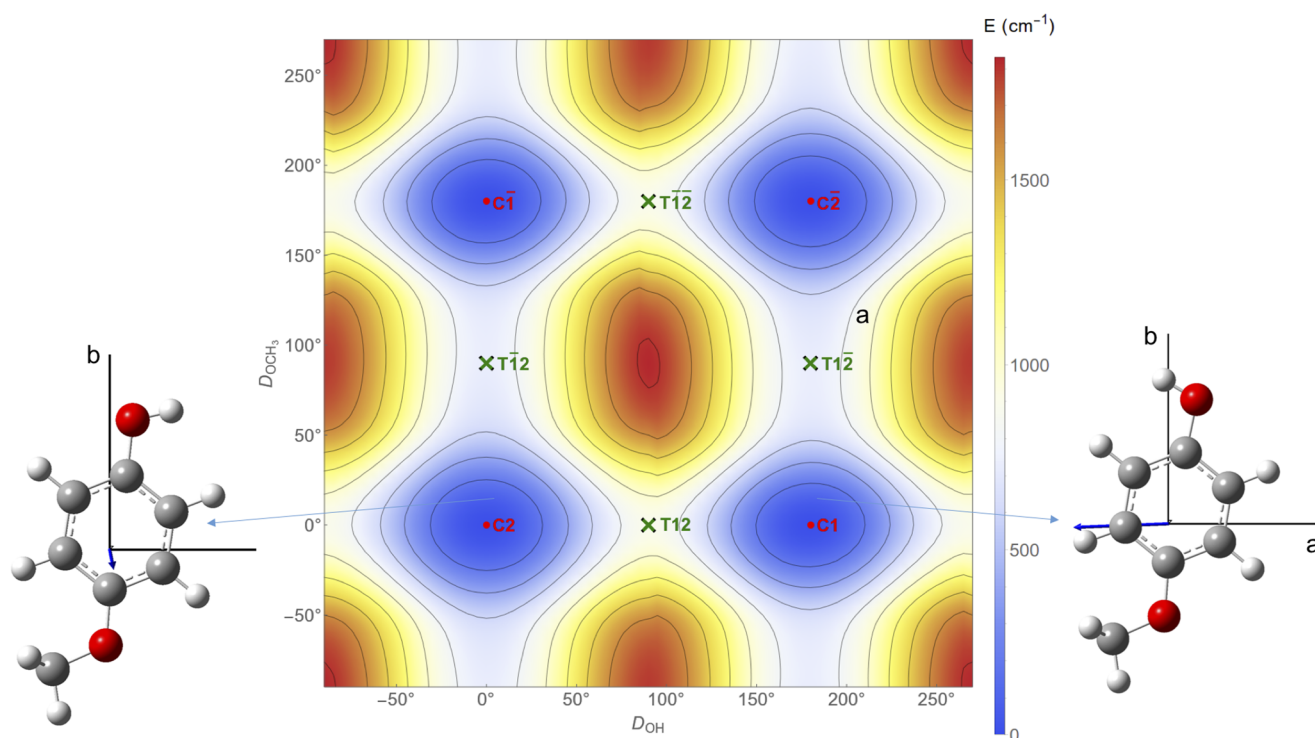


FIG. 4. PES describing the conformational space of 4-MP built with a step of 5° at the B3LYP/6-311++G(d,p) level of theory. Local minima and saddle points are, respectively, marked with a red dot and a green cross. Geometries of C1 and C2 stable conformers are optimized at the B3LYP/cc-pVTZ level of theory shown in the ab plane with their permanent dipolar vectors (blue arrow).

2-MP is presented in Fig. 5. In agreement with the previous theoretical considerations, only the conformer C1, stabilised by the intramolecular HB, was observed in the rotational spectrum of 2-MP

measured between 70 and 330 GHz. Starting from the SPCAT simulations from the initial set of molecular parameters, the fit was iteratively extended up to J and K_a values equal to 167 and 79,

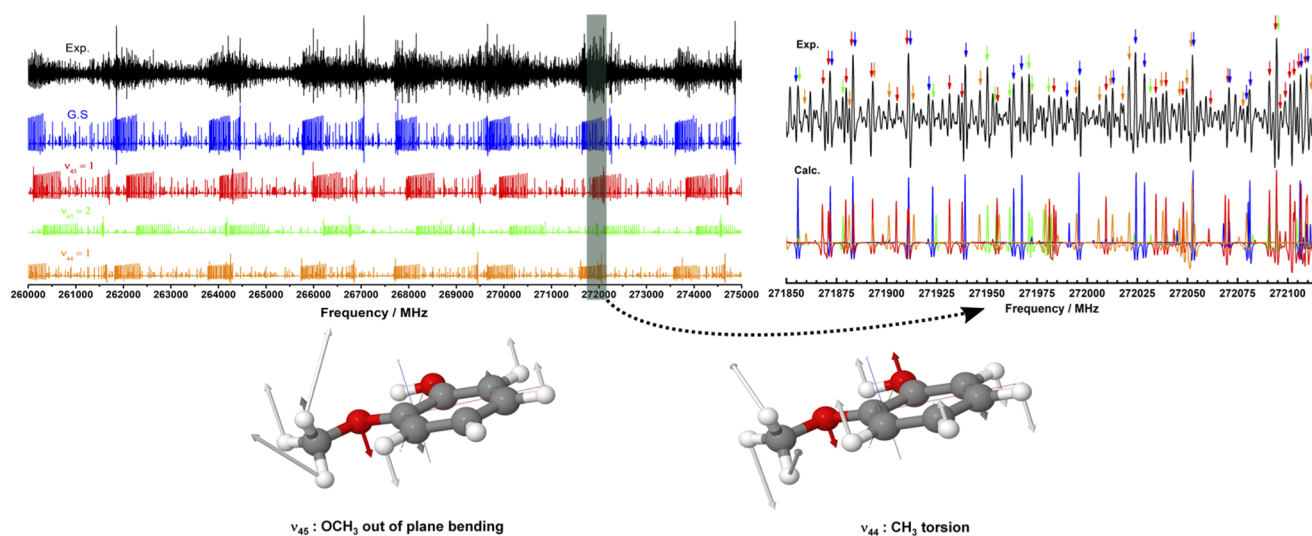


FIG. 5. Top: The experimental (in black) mm-wave spectrum (left: 260-275 GHz scan, right: zoom of 250 MHz) of 2-MP C1 is compared with the fitted spectra in color (GS in blue, vibrationally ES $v_{45} = 1$, $v_{45} = 2$ and $v_{44} = 1$ in red, green and orange, respectively). Bottom: description of the v_{45} and v_{44} vibrational modes.

TABLE II. Summary of the fitted parameters for 2-MP C1 and 4-MP C1 in the GS. The number N of assigned rotational lines in the fit as well as the maximum values of quantum numbers (J_{max} , K_{max}) and the standard deviations are indicated.

Parameter	Unit	This work mm-wave spectroscopy	Parameter	Unit	This work mm-wave spectroscopy
2-MP C1			4-MP C1		
A	MHz	2 607.062 60(117)	A	MHz	4 879.847 983(75)
B	MHz	1 560.796 45(40)	B	MHz	990.884 961(33)
C	MHz	982.871 842(199)	C	MHz	828.439 599 7(213)
Δ_J	kHz	0.054 708 8(185)	D_J	kHz	0.020 060 90(102)
Δ_K	kHz	0.192 821(310)	D_K	kHz	0.987 496(34)
Δ_{JK}	kHz	0.063 713(200)	D_{JK}	kHz	−0.037 464 3(65)
δ_J	Hz	19.811 2(89)	d_1	Hz	−4.194 03(59)
δ_K	Hz	111.528(86)	d_2	Hz	−0.341 409(228)
N_{a-type}		6 657	N_{a-type}		0
N_{b-type}		5 215	N_{b-type}		6 076
J_{max}		167	J_{max}		196
K_{max}		79	K_{max}		42
rms	kHz	88.2	rms	kHz	83.1
Unitless rms		1.02	Unitless rms		1.05

respectively. In total, around 12 000 lines were assigned to GS rotational transitions shared as *a*- and *b*-type according to the calculated dipole moment orientation. Pure rotational constants *A*, *B*, and *C* were carried out at the kHz level with higher accuracy compared to Ref. 6 and the complete set of quartic centrifugal distortion constants (Δ_J , Δ_K , Δ_{JK} , δ_J , and δ_K) were well determined to reproduce the measured transitions at the experimental accuracy (see Table II).

The same assignment procedure was undertaken for 4-MP. Nevertheless, compared to 2-MP, the assignment of 4-MP spectra was more difficult due, in part, to lower rotational absorptions/emissions essentially explained by a room temperature equilibrium vapour pressure 15 times weaker.¹⁰ An example of 4-MP mm-wave rotational spectrum and its assignment is presented in Fig. 6. As it was expected by the theoretical analysis (see Sec. III A), only the *cis*-rotamer (4-MP C1) was assigned in the experimental spectra and the *trans* conformation (4-MP C2) was not observed. Indeed, in addition to the low vapour pressure of 4-MP, the weak polarity of the *trans*-rotamer (see Table I: $\left(\frac{\mu_{b,A-4-MP\ C1}}{\mu_{a,A-4-MP\ C2}}\right)^2 \simeq 30$) prevents its observation in our experimental conditions. Therefore, the 4-MP mm-wave spectra exhibit only rotational transitions of the *cis*-rotamer (4-MP C1). Starting from the scaled B3LYP/cc-pVTZ rotational constants,²⁸ the GS *b*-type rotational transitions of 4-MP C1 were straightforwardly assigned and its molecular parameters fitted at the experimental accuracy (see Table II). Compared to 2-MP, the same degree of accuracy is reached on the rotational and quartic centrifugal distortion constants with more than 6000 *b*-type transitions assigned and a global rms close to 80 kHz. Even with the observation of a unique conformer, a lot of lines remain unassigned after the GS analysis, which indicates the large contribution of pure rotational transitions in the vibrational ES.

2. Vibrationally ES analysis

In the case of 2-MP, following the successful analysis of the GS, numerous remaining lines were assigned to pure rotational transitions in the vibrationally ES populated at room temperature. Three sets of ES molecular parameters were included in a global fit procedure to assign all the rotational structures by comparing the experimental and calculated spectra from the fitted parameters (Fig. 5). The assigned vibrationally ES are located below 200 cm^{-1} and correspond to the three lowest energy vibrations. Using the FT Far-IR synchrotron middle-resolution measurements of Cuisset *et al.* in Ref. 29 and the B3LYP/cc-pVTZ anharmonic frequencies of the 2-MP C1 rotamer, the three lowest vibrational levels have been identified: the first level is the fundamental $\nu_{45} = 1$ methoxy out of plane bending; the second level is its overtone $\nu_{45} = 2$ and the third level is the methyl torsion fundamental $\nu_{44} = 1$ (experimental and calculated harmonic and anharmonic frequencies are listed in Table III). An initial set of spectroscopic parameters for these ES were calculated from calculated anharmonic corrections and scaled with a factor corresponding to the ratio between experimental and calculated rotational constants in the GS.²⁸ All the fitted spectroscopic parameters resulting from the global fit are summarized in Table III. As for the GS, pure rotational constants were carried out at the kHz level and the complete set of quartic centrifugal distortion constants were well determined to reproduce the measured transitions at the experimental accuracy. Near 20 000 lines of the 2-MP spectra have been assigned to *a*-type and *b*-type pure rotational transitions in the low-energy vibrationally ES.

The vibrationally ES analysis of 4-MP C1 was performed identically to 2-MP C1. As for 2-MP, pure rotational transitions in the $\nu_{45} = 1$, $\nu_{45} = 2$, and $\nu_{44} = 1$ were identified. The results are presented in the second part of Table III. Unlike 2-MP, the lowest energy

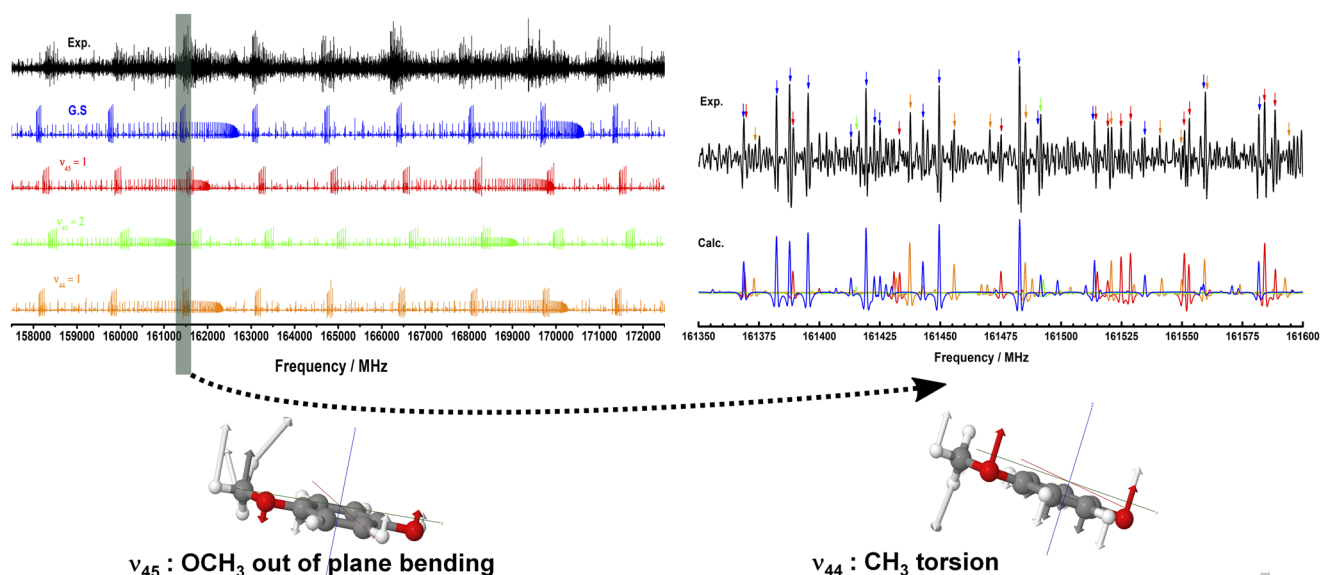


FIG. 6. Top: The experimental (in black) mm-wave spectrum (left: 157-173 GHz scan, right: zoom of 250 MHz) of 4-MP C1 is compared with the fitted spectra in color (GS in blue, vibrationally ES $\nu_{45} = 1$, $\nu_{45} = 2$, and $\nu_{44} = 1$ in red, green and orange, respectively). Bottom: description of the ν_{45} and ν_{44} vibrational modes.

vibrational band of 4-MP was not observed in the FT-Far-IR gas phase spectra of Ref. 27. The B3LYP/cc-pVTZ anharmonic frequency calculation has predicted the ν_{45} fundamental mode at 66.5 cm^{-1} red-shifted compared to the one of 2-MP C1 whereas the ν_{44} of 4-MP is blue-shifted. As in 2-MP, all the rotational constants in $\nu_{45} = 1$ ES were correctly determined with a comparable degree of accuracy. For $\nu_{45} = 2$ and $\nu_{44} = 1$, weaker intensity rotational lines complicate the assignment and it was not possible to reach the same fit quality with larger values of the rms. Compared to the other vibrationally ES analyses, we cannot exclude here a possible overlap of the rotational structures of $\nu_{45} = 2$ and $\nu_{44} = 1$ taking into account the rather close vibrational frequencies calculated at the B3LYP/cc-pVTZ level of theory. In our case, the isolated state model turned out to be adequate within the accuracy of our data for 2-MP and 4-MP except for the two previously mentioned states. A specific treatment of the perturbation by the introduction of interaction terms is in this case required if a sufficient level mixing is reached.⁴¹ The energy file generated by the SPCAT Pickett's program²¹ provides us the mixing coefficients P_{mix} of 4-MP rotational transitions in the $\nu_{45} = 2$ and $\nu_{44} = 1$ ES. Figure 7 shows the evolution of the mixing coefficient with the J'' and K_a'' quantum numbers for $\nu_{45} = 2$ (red circles) and $\nu_{44} = 1$ (black circles) ES. This figure highlights a strong perturbation between the two ES with important level mixing ($P_{mix} > 5\%$) for high J'' and K_a'' values ($J'' \approx K_a'' > 120$). In our case, due to a limited sensitivity, only transitions with $K_a'' < 34$ may be assigned and it was not possible to improve the quality of the fit by adding perturbation parameters such as b -type Coriolis interaction terms in the global fit.

C. Inertial defects

The inertial defect ΔI in $\text{amu}\cdot\text{\AA}^2$ units is a molecular parameter directly determined from the principal moments of inertia

I_α ($\alpha = a, b, c$) or from the rotational constants A, B, C in MHz using the relation

$$\Delta I = I_c - I_b - I_a = \frac{h}{8\pi^2} \left(\frac{1}{C} - \frac{1}{B} - \frac{1}{A} \right) \quad (1)$$

with $\frac{h}{8\pi^2} = 5.05379 \times 10^5 \text{ amu}\cdot\text{\AA}^2\cdot\text{MHz}$. ΔI is very nearly 0 for a planar molecule and is negative for non-planar molecules.⁴² Therefore, the value of the inertial defect is in general used in rotationally resolved spectroscopy to probe the degree of non-planarity of a molecule.

1. GS inertial defects

Several groups worked on the determination of a general formula providing the inertial defect of planar molecules with very low out-of-plane vibrations: in particular, Morino and Oka have generalised the expression of ΔI for any planar asymmetric top.⁴³ All these studies provided theoretical values of the GS ΔI in very good agreement with rotationally resolved measurements. Moreover, with the increasing quantity of high-resolution GS data on benzene derivatives and polycyclic aromatic compounds exhibiting a slight negative inertial defect, several authors have determined semi-empirical relations between the inertial defect ΔI , the wavenumber of the lowest out-of-plane vibration ν_l , and the square root of the c -axis principal moment of inertia $\sqrt{I_c}$.^{42,44,45}

In the context of the MP study, we have identified in the literature GS rotationally resolved measurements on phenol and anisole derivatives for which all isomers were studied. Table IV compares the GS inertia defects of ortho, meta, and para isomers of phenol and anisole derivatives in order to explain negative inertial defects of methoxyphenol isomers. The main contribution to the non-planarity and to the negative ΔI of MP comes from the out of plane hydrogen atoms in the methoxy

TABLE III. Summary of the fitted parameters in the vibrationally ES for 2-MP C1 and 4-MP C1. Experimental vibrational wavenumbers from Ref. 29 and rotational constants fitted in this study are compared with B3LYP/cc-pVTZ anharmonic calculations. The number N of assigned rotational lines in the fit as well as the maximum values of quantum numbers (J_{max} , K_{max}) and the standard deviations are indicated.

	Parameter	Expt.	Calc.	Expt.	Calc.	Expt.	Calc.
2-MP C1		$v_{45} = 1$		$v_{45} = 2$		$v_{44} = 1$	
	$\nu_{harm}/\text{cm}^{-1}$		77.0		154.0		178.6
	$\nu_{anharm}/\text{cm}^{-1}$	63.5	76.2		152.0		105.8
	A/MHz	2 605.452 91(106)	2604.72	2 604.068 62(201)	2603.43	2 604.999 2(34)	2603.46
	B/MHz	1 560.524 61(58)	1541.35	1 560.178 05(246)	1540.90	1 559.269 02(226)	1540.27
	C/MHz	984.254 416(198)	976.45	985.681 371(312)	977.77	983.123 26(35)	975.34
	$\Delta I/\text{amu}\cdot\text{\AA}^2$	-4.357 93(30)	-4.339	-5.276 32(82)	-5.229	-4.061 72(91)	-4.074
	$\Delta J/\text{kHz}$	0.055 918(41)		0.0571 77(82)		0.055 106(264)	
	$\Delta K/\text{kHz}$	0.194 528(245)		0.192 65(34)		0.184 57(101)	
	Δ_{JK}/kHz	0.066 908(225)		0.071 95(33)		0.067 21(114)	
	δ_J/Hz	20.114 9(199)		20.384(42)		19.910(131)	
	δ_K/Hz	113.784(115)		115.327(216)		111.69(57)	
	N_{a-type}	5 051		2 766		1 930	
	N_{b-type}	4 144		2 866		2 023	
	J_{max}	166		166		165	
	K_{max}	88		60		60	
	rms/kHz	92.6		89.6		83.0	
Unitless rms	1.13		1.14		1.21		
4-MP C1		$v_{45} = 1$		$v_{45} = 2$		$v_{44} = 1$	
	$\nu_{harm}/\text{cm}^{-1}$		81.0		162.0		156.2
	$\nu_{anharm}/\text{cm}^{-1}$		66.5		148.7		127.5
	A/MHz	4 864.772 323(86)	4887.01	4846.49574(59)	4870.67	4 872.252 01(111)	4892.73
	B/MHz	991.039 897(48)	980.50	991.25815(50)	980.74	990.708 00(90)	980.05
	C/MHz	829.410 452(33)	822.57	830.396 581(57)	823.50	828.849 041(81)	821.94
	$\Delta I/\text{amu}\cdot\text{\AA}^2$	-4.510 463(51)	-4.452	-5.51354(31)	-5.366	-4.109 10(55)	-4.0971
	D_J/kHz	0.020 466 53(163)		0.0206 232(113)		0.020 612 3(158)	
	D_K/kHz	1.005 240(42)		0.98844(38)		1.783 37(100)	
	D_{JK}/kHz	-0.040 977 7(85)		-0.052632(75)		-0.057 969(155)	
	d_1/Hz	-4.198 73(82)		-4.0490(78)		-4.333 4(109)	
	d_2/Hz	-0.322 90(36)		-0.30507(198)		-0.253 8(33)	
	N_{a-type}	0		0		0	
	N_{b-type}	4 508		1 093		965	
	J_{max}	188		190		175	
	K_{max}	41		35		27	
	rms/kHz	91.5		123.8		139.6	
Unitless rms	1.16		1.57		1.78		

group, while the -OH group does not induce a significant negative inertial defect. Therefore, the ΔI values of MP are slightly lower than the ΔI of cresol³⁶⁻³⁸ and anisole.³⁹ The ΔI values for MP/cresol and methylanisole/dimethoxybenzene^{24-26,40} indicate a stronger contribution on the negative inertial defects for the methoxy group compared to the methyl group, probably explained by the contribution of the OCH₃ out of plane contribution ($\nu_l = \nu_{45}$ for MP) leading to a slight negative zero point inertial defect.⁴⁴

Now, when we focus our attention on the isomeric dependence on the inertial defects, the most negative value is always obtained

for the para isomer and the ΔI value of the ortho isomer appears to be slightly lower than that of the meta isomer. From these observations, two complementary elements of explanation may be proposed: (i) the zero point inertial defect induced by the low-energy out of plane modes is favoured in para positions with the largest distance between the two functional groups; (ii) the isomeric dependence of ΔI is in agreement with the isomeric frequency dependence of ν_l ($\Delta I_{para} < \Delta I_{ortho} \leq \Delta I_{meta} \Leftrightarrow \nu_{l,para} < \nu_{l,ortho} \leq \nu_{l,meta}$). Finally, it can be noticed that the formation of the intramolecular HB between the -OH and the -OCH₃ functional group in 2-MP does not affect the inertial defect of 2-MP.

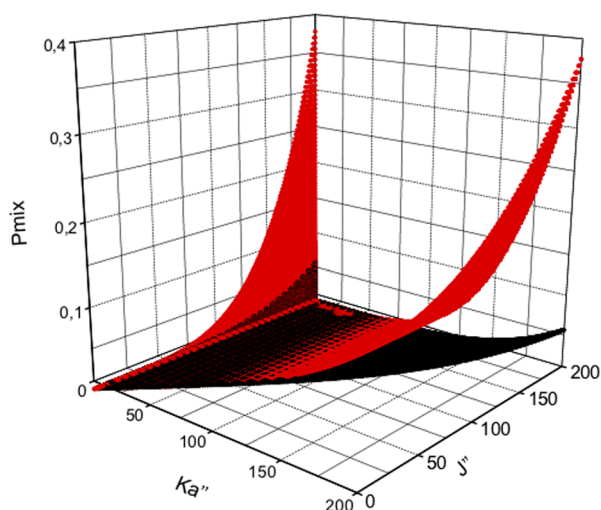


FIG. 7. 3D representation of the mixing coefficient P_{mix} of 4-MP rotational energy levels of the $v_{45} = 2$ (red circles) and $v_{44} = 1$ (black circles) ES vs the J'' and K_a'' quantum numbers. The values of P_{mix} were directly obtained from the .egy file generated by the SPCAT Pickett's program.²¹ Projections on the (P_{mix}, J'') and (P_{mix}, K_a'') planes are plotted.

2. ES inertial defects

In 1966, Hanyu *et al.*⁴⁶ observed the decreasing of the inertial defect of nitrosobenzene with each excitation of the low-frequency out of plane vibration ν_l . In a first approximation, they have demonstrated that if the lowest frequency out of plane vibration has an energy sufficiently lower than the higher energy in-plane modes ($\nu_s^2 \gg \nu_l^2$ see Refs. 42 and 46), then the variation of the inertial defects between two adjacent out of plane modes is given by

$$\Delta I_{\nu_l=n+1} - \Delta I_{\nu_l=n} = -\frac{h}{2\pi^2 c \nu_l} \quad (2)$$

with $\frac{h}{2\pi^2 c} = 67.4305 \text{ amu} \cdot \text{\AA}^2 \text{ cm}^{-1}$ and ν_l the lowest energy out of plane mode wavenumber in cm^{-1} .

TABLE IV. GS inertial defects in $\text{amu} \cdot \text{\AA}^2$ units of ortho, meta, and para isomers of phenol and anisole derivatives measured by rotationally resolved high resolution spectroscopy. Only the most stable observed rotamers have been considered.

Molecule	Functional groups	ΔI_{ortho}	ΔI_{meta}	ΔI_{para}	References
Methoxyphenol	OH/OCH ₃	-3.459	-3.428	-3.555	This work (ortho, para) + Ref. 9 (meta)
Phenol	OH		-0.031		Reference 30
Fluorophenol	OH/F	0.002	-0.017	-0.073	Reference 31 (ortho, meta) + Ref. 32 (para)
Dihydroxybenzene	OH/OH	-0.094	-0.083	-0.159	Reference 33 (ortho) + Ref. 34 (meta) + Ref. 35 (para)
Cresol	OH/CH ₃	-3.230	-3.156	-3.253	Reference 36 (ortho) + Ref. 37 (meta) + Ref. 38 (para)
Anisole	OCH ₃		-3.409		Reference 39
Methylanisole	OCH ₃ /CH ₃	-6.729	-6.600	-6.733	Reference 24 (ortho) + Ref. 25 (meta) + Ref. 26 (para)
Dimethoxybenzene	OCH ₃ /OCH ₃	-6.777	-6.777	-6.952	Reference 40

TABLE V. Variation of the inertial defects $\Delta I_{\nu_{45}=2} - \Delta I_{\nu_{45}=1}$ in $\text{amu} \cdot \text{\AA}^2$ units with the excitation of the lowest energy out of plane vibrational mode ν_{45} . Comparison of the vibrational wavenumbers $\nu_{45} = 1$ in cm^{-1} unit deduced from Eq. (2) $\nu_{45, \Delta I} = 1$,^{42,46} the experimental value $\nu_{45, exp.} = 1$ obtained in Ref. 29 by FT-Far-IR spectroscopy and anharmonic calculations $\nu_{45, calc.} = 1$ at the B3LYP/cc-pVTZ level of theory.

Molecule	$\Delta I_{\nu_{45}=2} - \Delta I_{\nu_{45}=1}$	$\nu_{45, \Delta I} = 1$ ^{42,46}	$\nu_{45, exp.} = 1$ ²⁹	$\nu_{45, calc.} = 1$
2-MP C1	-0.918 39	73.4	63.5	76.2
3-MP C2 ⁹	-0.876 87	76.9	78.3	80.2
4-MP C1	-1.003 08	67.2	...	66.5

As shown in Table III, the rotational constants of $\nu_{45} = 2$ and $\nu_{44} = 1$ ES (especially for 2-MP) are very close. That is not the case for their inertia defects with a value of $\Delta I_{\nu_{45}=2}$ significantly lower than the $\Delta I_{\nu_{44}=1}$ value according to Eq. (2), which ensures the validity of our assignment. In the other hand, it was possible to determine from the rotational constants the vibrational wavenumbers of $\nu_{45} = 1$ for the three MP isomers by using Eq. (2) of Hanyu *et al.*⁴⁶ The results are presented in Table V where the variation of the inertial defects $\Delta I_{\nu_{45}=2} - \Delta I_{\nu_{45}=1}$ in $\text{amu} \cdot \text{\AA}^2$ units with the excitation of the lowest energy out of plane vibrational mode ν_{45} has been calculated for 2-MP C1, 3-MP C2,⁹ and 4-MP C1. Taking into account the good precision of the ES ΔI measured by mm-wave spectroscopy, this variation is determined with a high degree of accuracy and the isomeric order discussed in Sec. III C 1 is again verified ($\Delta I_{\nu_{45}=2} - \Delta I_{\nu_{45}=1})_{para} < (\Delta I_{\nu_{45}=2} - \Delta I_{\nu_{45}=1})_{ortho} < (\Delta I_{\nu_{45}=2} - \Delta I_{\nu_{45}=1})_{meta}$. Using Eq. (2), it was possible to determine, from negative inertial defects, the lowest energy out of plane mode wavenumber noted $\nu_{45, \Delta I}$ in Table V and to compare the obtained values with experimental FT-Far-IR²⁹ and calculated B3LYP/cc-pVTZ vibrational wavenumbers. For 2-MP C1 and 3-MP C2, the agreement of $\nu_{45, \Delta I}$ values and the experimental measurements is better than 10 cm^{-1} . In the case of 4-MP, the variation of the inertial defects with the excitation of the ν_{45} mode allows us to estimate the position of the non-observed vibrational band center at 67.2 cm^{-1} in very good agreement with the anharmonic calculated value of 66.5 cm^{-1} .

IV. CONCLUSIONS

Millimetre-wave absorption and emission rotational spectra of guaiacol (2-MP) and mequinol (4-MP) have been measured with a frequency multiplication chain and a mm-wave CPFT spectrometer, respectively. The experimental measurements were supplemented by anharmonic B3LYP/cc-pVTZ calculations. For 2-MP, only one rotamer may be observed at room temperature in the mm-wave spectra. This conformation is strongly stabilised by the formation of an intramolecular O–H...OCH₃ HB characterised in this work by a topology analysis of the electron density. The full set of GS molecular parameters including quartic corrections has been fitted allowing to reproduce *a*-type and *b*-type rotational transitions at the experimental accuracy. In a global fit including more than 30 000 lines, pure rotational transitions in three ES have been assigned and the corresponding molecular constants fitted. These ES correspond to the fundamental and the overtone of the ν_{45} out of plane O–CH₃ bending and the fundamental ν_{44} CH₃ torsion. For 4-MP, two stable rotamers, one in configuration *cis* and the other one in configuration *trans* were expected. Due to the weak polarity of the *trans* structure, only the *cis*-rotamer was observed in the mm-wave spectra. As for 2-MP, both GS and the three previously mentioned ES were assigned and all the molecular parameters up to quartic corrections were determined. Nevertheless, for $\nu_{45} = 2$ and $\nu_{44} = 1$ ES, an interaction between the two ES was highlighted at high J'' and K_a'' values. We have additionally discussed the negative inertial defects of the three MP isomers. A comparison of different phenol and anisole derivatives highlights an isomeric dependence of the GS ΔI according to the lowest vibrational energies of the out of plane modes. The measured ΔI allowed to avoid any ambiguity in the low-frequency vibrational ES assignment. The variation of the inertial defects with the excitation of the methoxy out of plane mode allows us to estimate with a good degree of accuracy its vibrational energy. All these results demonstrate that the negative inertial defect of aromatic compounds, measured with a sufficient precision, is a powerful tool to discriminate isomers and to assign unambiguously the rotational structures in the low-energy out of plane vibrational states. An improvement of the sensitivity of the spectrometers should allow in the near future to study the weakly volatile syringol, the other primary block of lignin released in quantity in the atmosphere during biomass fires.⁴⁷ Finally, microwave, THz and IR spectrometers coupled to free jet supersonic beams suggest the possibility to study hydrated MP complexes as it was performed with the benzoic acid-water complex in order to bridge the gap between gas-phase and aerosols in the atmosphere towards the study of micro-solvation processes.⁴⁸

SUPPLEMENTARY MATERIAL

The line lists of the assigned mm-wave rotational transitions frequencies of 2-MP and 4-MP in the GS and ES are, respectively, presented in Tables S1 and S2 of the [supplementary material](#).

ACKNOWLEDGMENTS

This work and the postdoc of A. Jabri took place in the Labex CaPPA (Chemical and Physical Properties of the Atmosphere) funded by the French National Research Agency (ANR) through the PIA (Programme d'Investissements d'Avenir) under Contract

No. ANR-11-LABX-005-01. The Ph.D. of A. Roucou was supported by the Région Hauts-de-France and the French Direction Générale de l'Armement (DGA). The authors are also grateful for the financial grant received from the Région Hauts-de-France, the Ministère de l'Enseignement Supérieur et de la Recherche (CPER Climibio), and the European Fund for Regional Economic Development. ANR is also thanked for their financial support for the project Original Sub-millimetre Chirped pulse instrumentation for Astrochemical Reactivity (OSCAR) under Contract No. ANR-15-CE29-0017. The last acknowledgements go to two computational clusters: the Centre de Ressources Informatiques de Lille 1 (CRI) and CAL-CULCO, the computing platform from the Université du Littoral Côte d'Opale where the GAUSSIAN16 and MOLPRO calculations were performed, respectively.

REFERENCES

- C. D. Simpson, M. Paulsen, R. L. Dills, L.-J. S. Liu, and D. A. Kalman, *Environ. Sci. Technol.* **39**, 631–637 (2005).
- A. Lauraguais, C. Coeur-Tourneur, A. Cassez, K. Deboudt, M. Fourmentin, and M. Choël, *Atmos. Environ.* **86**, 155–163 (2014).
- W. Ahmad, C. Coeur, A. Tomas, T. Fagniez, J.-B. Brubach, and A. Cuisset, *Appl. Opt.* **56**, E116–E122 (2017).
- S. Islam, A. Ganesan, R. Auchettl, O. Plekan, R. G. Acres, F. Wang, and K. C. Prince, *J. Chem. Phys.* **149**, 134312 (2018).
- W. Caminati, S. Melandri, and L. B. Favero, *J. Mol. Spectrosc.* **161**, 427–434 (1993).
- J. A. Ruiz-Santoyo, M. Rodríguez-Matus, J. L. Cabellos, J. T. Yi, D. W. Pratt, M. Schmitt, G. Merino, and L. Álvarez-Valtierra, *J. Chem. Phys.* **143**, 094301 (2015).
- S. Ullrich, W. D. Geppert, C. E. Dessent, and K. Müller-Dethlefs, *J. Phys. Chem. A* **104**, 11864–11869 (2000).
- M. Wilke, M. Schneider, J. Wilke, J. A. Ruiz-Santoyo, J. J. Campos-Amador, M. E. González-Medina, L. Álvarez-Valtierra, and M. Schmitt, *J. Mol. Struct.* **1140**, 59–66 (2017).
- A. Roucou, D. Fontanari, G. Dhont, A. Jabri, C. Bray, F. Hindle, G. Mouret, R. Bocquet, and A. Cuisset, *ChemPhysChem* **19**, 1572–1578 (2018).
- S. Kim, P. A. Thiessen, E. E. Bolton, J. Chen, G. Fu, A. Gindulyte, L. Han, J. He, S. He, B. A. Shoemaker *et al.*, *Nucleic Acids Res.* **44**, D1202–D1213 (2015).
- G. Mouret, M. Guinet, A. Cuisset, L. Croize, S. Eliet, R. Bocquet, and F. Hindle, *IEEE Sens. J.* **13**, 133–138 (2013).
- F. Hindle, C. Bray, K. Hickson, D. Fontanari, M. Mouelhi, A. Cuisset, G. Mouret, and R. Bocquet, *J. Infrared, Millimeter, Terahertz Waves* **39**, 105–119 (2018).
- A. M. Daly, L. Kolesnikova, S. Mata, and J. L. Alonso, *J. Mol. Spectrosc.* **306**, 11–18 (2014).
- M. Martin-Drumel, F. Hindle, G. Mouret, A. Cuisset, and J. Cernicharo, *Astrophys. J.* **799**, 115 (2015).
- J. L. Neill, B. J. Harris, A. L. Steber, K. O. Douglass, D. F. Plusquellic, and B. H. Pate, *Opt. Express* **21**, 19743–19749 (2013).
- M. Frisch, G. Trucks, H. Schlegel, G. Scuseria, M. Robb, J. Cheeseman, G. Scalmani, V. Barone, G. Petersson, H. Nakatsuji *et al.*, Gaussian 16, Revision a. 03, Gaussian, Inc., Wallingford, CT, 2016.
- R. A. Kendall, T. H. Dunning, Jr., and R. J. Harrison, *J. Chem. Phys.* **96**, 6796–6806 (1992).
- L. Cesari, L. Canabady-Rochelle, and F. Mutelet, *Struct. Chem.* **29**, 179–194 (2018).
- H.-J. Werner, P. J. Knowles, G. Knizia, F. R. Manby, and M. Schütz, *Wiley Interdiscip. Rev.: Comput. Mol. Sci.* **2**, 242–253 (2012).
- T. Lu and F. Chen, *J. Comput. Chem.* **33**, 580–592 (2012).
- H. M. Pickett, *J. Mol. Spectrosc.* **148**, 371–377 (1991).
- Z. Kisiel, E. Białkowska-Jaworska, and L. Pszczółkowski, *J. Chem. Phys.* **109**, 10263–10272 (1998).

- ²³Z. Kisiel, E. Białkowska-Jaworska, and L. Pszczółkowski, *J. Mol. Spectrosc.* **199**, 5–12 (2000).
- ²⁴L. Ferres, H. Mouhib, W. Stahl, and H. V. L. Nguyen, *ChemPhysChem* **18**, 1855–1859 (2017).
- ²⁵L. Ferres, W. Stahl, and H. V. L. Nguyen, *J. Chem. Phys.* **148**, 124304 (2018).
- ²⁶L. Ferres, W. Stahl, I. Kleiner, and H. V. L. Nguyen, *J. Mol. Spectrosc.* **343**, 44–49 (2018).
- ²⁷A. Cuisset, M.-A. M. Drumel, F. Hindle, G. Mouret, and D. A. Sadovskii, *Chem. Phys. Lett.* **586**, 10–15 (2013).
- ²⁸A. Roucou, G. Dhont, A. Cuisset, M.-A. Martin-Drumel, S. Thorwirth, D. Fontanari, and W. L. Meerts, *J. Chem. Phys.* **147**, 054303 (2017).
- ²⁹A. Cuisset, C. Coeur, G. Mouret, W. Ahmad, A. Tomas, and O. Pirali, *J. Quant. Spectrosc. Radiat. Transfer* **179**, 51–58 (2016).
- ³⁰C. Tanjaroon and S. G. Kukulich, *J. Phys. Chem. A* **113**, 9185–9192 (2009).
- ³¹A. Bell, J. Singer, D. Desmond, O. Mahassneh, and J. van Wijngaarden, *J. Mol. Spectrosc.* **331**, 53–59 (2017).
- ³²C. Ratzer, M. Nispel, and M. Schmitt, *Phys. Chem. Chem. Phys.* **5**, 812–819 (2003).
- ³³W. Caminati, S. Di Bernardo, L. Schäfer, S. Q. Kulp-Newton, and K. Siam, *J. Mol. Struct.* **240**, 263–274 (1990).
- ³⁴S. Melandri, G. Maccaferri, W. Caminati, and P. G. Favero, *Chem. Phys. Lett.* **256**, 513–517 (1996).
- ³⁵W. Caminati, S. Melandri, and L. B. Favero, *J. Chem. Phys.* **100**, 8569–8572 (1994).
- ³⁶A. Welzel, A. Hellweg, I. Merke, and W. Stahl, *J. Mol. Spectrosc.* **215**, 58–65 (2002).
- ³⁷A. Hellweg, C. Hättig, I. Merke, and W. Stahl, *J. Chem. Phys.* **124**, 204305 (2006).
- ³⁸A. Hellweg and C. Hättig, *J. Chem. Phys.* **127**, 024307 (2007).
- ³⁹B. Reinhold, I. Finneran, and S. Shipman, *J. Mol. Spectrosc.* **270**, 89–97 (2011).
- ⁴⁰M. Schneider, M. Wilke, M.-L. Hebestreit, C. Henrichs, W. L. Meerts, and M. Schmitt, *ChemPhysChem* **19**, 307–318 (2018).
- ⁴¹O. Pirali, Z. Kisiel, M. Goubet, S. Gruet, M. Martin-Drumel, A. Cuisset, F. Hindle, and G. Mouret, *J. Chem. Phys.* **142**, 104310 (2015).
- ⁴²T. Oka, *J. Mol. Struct.* **352**, 225–233 (1995).
- ⁴³T. Oka and Y. Morino, *J. Mol. Spectrosc.* **6**, 472–482 (1961).
- ⁴⁴S. Gruet, M. Goubet, and O. Pirali, *J. Chem. Phys.* **140**, 234308 (2014).
- ⁴⁵M. K. Jahn, J.-U. Grabow, M. J. Travers, D. Wachsmuth, P. D. Godfrey, and D. McNaughton, *Phys. Chem. Chem. Phys.* **19**, 8970–8976 (2017).
- ⁴⁶Y. Hanyu, C. O. Britt, and J. E. Boggs, *J. Chem. Phys.* **45**, 4725–4728 (1966).
- ⁴⁷J. D. Young, M. Staniforth, J. C. Dean, G. M. Roberts, F. Mazzoni, T. N. Karsili, M. N. Ashfold, T. S. Zwier, and V. G. Stavros, *J. Phys. Chem. Lett.* **5**, 2138–2143 (2014).
- ⁴⁸E. G. Schnitzler and W. Jäger, *Phys. Chem. Chem. Phys.* **16**, 2305–2314 (2014).
- ⁴⁹A. Roucou, I. Kleiner, M. Goubet, S. Bteich, G. Mouret, R. Bocquet, F. Hindle, W. L. Meerts, and A. Cuisset, *ChemPhysChem* **19**, 1056–1067 (2018).